StrucOpt manuscript No.
(will be inserted by the editor)

Concurrent Performance and Manufacturing Cost Optimization of Structural Components*

W. D. Nadir, I. Y. Kim*, and O. L. de Weck

Abstract This paper presents a structural shape optimization method that considers not only structural performance but also manufacturing cost. Typical structural design optimization involves the optimization of important structural performance metrics such as stress, mass, deformation, or natural frequencies. Often factors such as manufacturing cost are not considered in structural optimization. In this paper, manufacturing cost is an important performance metric along with typical structural performance metrics. The trade-off between manufacturing cost and structural performance is observed in two examples using the manufacturing process of abrasive waterjet (AWJ) cutting.

Key words Cost modeling, multi-objective optimization, abrasive waterjet

Accepted: July 29, 2005

W. D. Nadir, I. Y. Kim, and O. L. de Weck

Department of Aeronautics & Astronautics, Room 33-409, Massachusetts Institute of Technology, Cambridge, Massachusetts 02139, USA
e-mail: bnadir@alum.mit.edu, e-mail: iykim@me.queensu.ca and e-mail: deweck@mit.edu

Send offprint requests to: William D. Nadir

* Presented as paper AIAA–2004–4593 at the 10th AIAA-ISSMO Multidisciplinary Analysis and Optimization Conference, Albany, New York, August 30-September 1, 2004

* *Present address:* Dept. of Mechanical Engineering, Queen's University, Kingston, Ontario, K7L 3N6, Canada

Nomenclature

C	=	Abrasive waterjet (AWJ) cutting speed estimation constant
C_{man}	=	Total manufacturing cost, USD
d_m	=	Mixing tube diameter of the AWJ cutting machine, in
d_o	=	AWJ cutter orifice diameter, in
E	=	AWJ cutter error limit
f_a	=	Abrasive factor for abrasive used in AWJ cutter
h	=	Thickness of material machined by AWJ, cm
J	=	Objective function
$\mathbf{L_j}$	=	Step length for j^{th} step along cut curve
m	=	Number of curves being optimized in the structure
M	=	Mass, kg
M_a	=	AWJ abrasive flow rate, lb/min
N_m	=	Machinability Number
OC	=	Overhead cost for machine shop, $/hr
P_w	=	AWJ water pressure, ksi
q	=	AWJ cutting quality
R	=	Arc section cut radius for AWJ cutter, in
$\mathbf{s_i}$	=	Total number of steps along i_{th} cutting curve
u_{max}	=	AWJ maximum linear cutting speed approximation, in/min
$\mathbf{x}$	=	X-coordinate design variable vector
$\mathbf{y}$	=	Y-coordinate design variable vector
α	=	Objective function weighting factor
δ	=	Deflection, mm
σ	=	Stress, Pa

1 Introduction and Literature Review

Typical structural design optimization involves the optimization of important structural performance metrics such as stress, mass, deformation, or natural frequencies. This structural design method often does not consider an important factor in structural design: manufacturing cost. In this research, manufacturing cost is an important

performance metric in addition to typical structural performance metrics. The weighted sum method by Zadeh (1963), is used to observe the trade-off between manufacturing cost and structural performance. Two examples are presented which exhibit this trade-off. These examples involve optimization of two-dimensional metallic structural parts: a generic part and a bicycle frame-like part.

While it is not possible to construct a manufacturing cost model that represents all manufacturing processes, the scope of this research has been limited to one manufacturing process: rapid prototyping using an abrasive water jet (AWJ) cutter. Although AWJ cutting is the only manufacturing process considered, this framework is generalizable to other manufacturing processes provided that realistic parametric cost models of the manufacturing process can be created and verified.

1.1 Literature review

The aim of structural optimization is to determine the values of structural design variables which minimize an objective function chosen by the designer for a structure while satisfying given constraints. Structural optimization may be subdivided into shape optimization and topology optimization. For shape optimization, the theory of shape design sensitivity analysis was established by Zolésio (1981) and Haug (1986). Bendsøe and Kikuchi (1988) and Suzuki and Kikuchi (1991) proposed the homogenization method for structural topology optimization by introducing microstructures and applied it to a variety of problems. Yang and Chuang (1994) proposed artificial material and used mathematical programming for topology optimization. Kim and Kwak (2002) first proposed design space optimization, in which the number of design variables and layout change during the course of optimization. Kim and de Weck (2005) developed a genetic algorithm in which the chromosome length changes as optimization progresses and applied the method to structural topology optimization problems.

Structural shape optimization has been performed along with an estimation of manufacturing cost by Chang and Tang (2001). This work involved optimization of a three-dimensional part in order to reduce mass and manufacturing cost for the special application of the fabrication of a mold or die. However, manufacturing cost was not included in either the objective or constraint function, as is done in this paper. Park (2004) performed optimization of composite structural design considering mechanical performance and manufacturing cost. This work focused on the optimal stacking sequence of composite layers as well as the optimal injection gate location to be used in the composite material manufacturing process, but also did not perform multidisciplinary optimization including manufacturing cost. Martinez (2001) and Curran (2005) performed optimization considering structural performance and manufacturing cost. Their cost models are based on empirical data, not a theoretical model as in this paper. In addition, their design variables consisted of component sizes and section properties while we change the structural shape using spline curves, allowing for significantly more design freedom.

The weighted sum method is a popular method for handling multi-objective problems. Zadeh (1963) performed early work on the weighted sum method. In addition, Koski (1988) used the weighted sum method for the application of multicriteria truss optimization.

The standard method for determining manufacturing cost for the AWJ manufacturing process is presented by Zeng (1993) as well as Singh and Munoz (1993). To estimate manufacturing cost, Zeng (1993) use the cutting speed of the water jet cutter to estimate cost via the required cutting length and layout.

AWJ cutting speed prediction models have been presented by Zeng (1999). Zeng and Kim developed a widely accepted AWJ cutting speed prediction model. In addition, Zeng (1992) developed the theory behind AWJ cutting process. Zeng et. al. (1992) conducted an experimental study to determine the machinability numbers of engineering materials used in water jet machining processes.

For the purposes of this paper, the AWJ cutting speed model presented by Zeng and Kim is used. The Zeng and Kim model has been used by Singh and Munoz to predict AWJ cutting speed and is also used in Omax water jet CAM software.

While other researchers have performed structural shape optimization and investigated manufacturing cost, a lack of research exists for true concurrent structural performance and manufacturing cost optimization of structural components with the use of spline curves for increased design freedom.

2 Optimization Framework

This section presents the optimization framework used to obtain an optimal structural design which meets the given design requirements. The modeling assumptions, optimization problem statement, optimization algorithm, and details of the software modules used in the simulation are presented.

2.1 Modeling assumptions

Several assumptions are made in the models for simplification. These are:

- The cuts made by the abrasive waterjet cutter for structural optimization example are closed curves.

– The cuts can not disappear or join together.
– The cuts can not intersect each other or the structural part boundary unless they define the part boundary.

These models were developed to investigate the trade-off between structural performance and manufacturing cost by incorporating a manufacturing cost model into a multi-objective optimization framework. These assumptions allowed for an exploration of the design space within a reasonable amount of time. More advanced models can be developed to allow for hole generation or merging, as done by Lee (2004).

2.2 Design objectives

Using the weighted sum method, the two considered design objectives are combined into a single objective function to minimize. The first design objective is structural performance defined as mass. The second is manufacturing cost.

$$J(x_j^i, y_j^i) = \alpha M + (1-\alpha) C_{man} \tag{1}$$

The objective function used for these simulations is shown in (1). In (1), J is the objective function, M is the structural mass, C_{man} is the total manufacturing cost of the structural component, x_j^i and y_j^i are the design vectors composed of the X and Y-coordinates of the j^{th} control point for the i^{th} Non-uniform rational b-spline (NURBS) curve, respectively, and α is the weighting factor for the two objectives.

NURBS, defined in Piegl and Tiller (1997), are used to describe the cut curves in the part. NURBS curves are chosen for their ability to control the shape of a curve on a local level by each of the defined control points, or knots. A complex shape can be represented with little data in the form of several of these control points.

2.3 Design variables

The design variables for the simulation are the X and Y coordinates of the control points defining the curves along which the abrasive waterjet cuts are made. Therefore, two design variables are required for each control point to define cuts in the component being optimized. The total number of design variables depends on the number of cutting curves and the number of control points used for each curve.

$$\mathbf{x} \equiv \left(\{x_1^1\}, \{x_2^1\}, \ldots, \{x_{n_1}^1\}, \ldots, \{x_1^m\}, \{x_2^m\}, \ldots, \{x_{n_m}^m\}\right) \tag{2}$$

$$\mathbf{y} \equiv \left(\{y_1^1\}, \{y_2^1\}, \ldots, \{y_{n_1}^1\}, \ldots, \{y_1^m\}, \{y_2^m\}, \ldots, \{y_{n_m}^m\}\right) \tag{3}$$

In (2) and (3), n_i is the total number of control points for the i^{th} curve and m is the total number of curves being optimized in the structure.

2.4 Design constraints

The constraints imposed on this problem statement are side constraints of the design variables and maximum von-Mises stress in the structure. These constraints are defined in the following equations.

$$\sigma_{max} \leq \sigma_c \tag{4}$$

$$x_{j,LB}^i \leq x_j^i \leq j, x_{UB}^i \tag{5}$$

$$y_{j,LB}^i \leq y_j^i \leq y_{j,UB}^i \tag{6}$$

In (4), (5), and (6), σ_{max} is the maximum von-Mises stress in the structure, σ_c is the maximum von-Mises stress constraint, and $x_{j,LB}^i$, $x_{j,UB}^i$, $y_{j,LB}^i$, and $y_{j,UB}^i$ are the lower (LB) and upper bound (UB) side constraints for the design vector variables controlling the j^{th} control point for the i^{th} NURBS curve. These side constraints are different for each design variable given the nature of the problems being optimized.

2.5 Flow chart

The optimal structural design for the given range of design requirements is determined using an optimization approach shown in Figure 1. A gradient-based optimizer is combined with a finite element analysis software module and an abrasive waterjet manufacturing cost estimation module to determine the optimal design solution.

The initial design, defined from X, Y coordinates and geometrical parameters, is input to the system and the objective function is evaluated using finite-element analysis with ANSYS 8.1 and the manufacturing cost estimation model. Rather than perform structural optimization and then off-line manufacturing cost evaluation, manufacturing cost and structural performance are both calculated simultaneously for each design from the optimizer. These designs are then evaluated based on their respective objective function values.

2.6 Gradient-based shape optimization

The optimization procedure used to optimize the shape of the cutting curves is performed using a gradient-based optimization algorithm, a MATLAB sequential quadratic programming optimization function, *fmincon*.

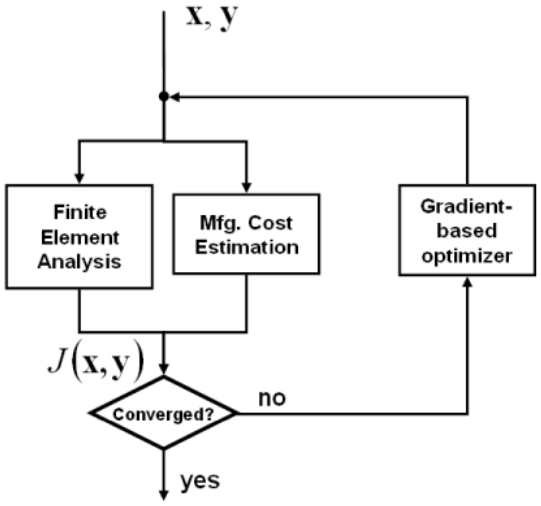

Fig. 1 Shape optimization flow chart.

2.7 Manufacturing cost estimation

This module is used to determine the manufacturing cost for performing abrasive waterjet manufacturing for structural components. The manufacturing process of abrasive waterjet cutting uses a powerful jet of a mixture of water and abrasive and a sophisticated control system combined with computer-aided machining (CAM) software. This provides for accurate movement of the cutting nozzle. The result is a machined part with tolerances ranging from ±0.001 to ±0.005 inches. It is possible for AWJ cutting machines to cut a wide range of materials including metals and plastics (Zeng et. al. (1992)).

The inputs to the AWJ manufacturing cost estimation module include design variables and parameters such as material properties, material thickness, and abrasive waterjet settings. The output of this module is the AWJ manufacturing cost and time to manufacture the structural design.

Based on the material thickness and material properties, a maximum cutting speed is determined for the AWJ cutting machine. While the cutting speed of the waterjet cutter is constant throughout most of the cutting operation for a sufficiently large cutting path radius of curvature, the cutting speed of waterjet slows if any sharp corners or curves with small arc radii lie along the cutting path. (7) is used to determine the maximum linear cutting speed of the AWJ cutter, u_{max}. The overhead cost associated with using the AWJ cutting machine, OC, is shown in (8). This cost factor is provided as an estimate of the manufacturing cost overhead for the MIT Department of Aeronautics and Astronautics machine shop.

$$u_{max} = \left(\frac{f_a N_m P_w^{1.594} d_o^{1.374} M_a^{0.343}}{C q h d_m^{0.618}} \right)^{1.15} \tag{7}$$

$$OC = \$75/hr \tag{8}$$

In (7) and (8), f_a is an abrasive factor, N_m is the machinability number of the material being machined, P_w is the water pressure, d_o is the orifice diameter, M_a is the abrasive flow rate, q is the user-specified cutting quality, h is the material thickness, d_m is the mixing tube diameter, and C is a system constant that varies depending on whether metric or Imperial units are used (Zeng (1993)). The AWJ settings used for this simulation are shown in Table 1.

AWJ Setting	Value
Abrasive factor, f_a	1
Machinability number, N_m	87.6
Water pressure, P_w	40
Orifice diameter, d_o	0.014
Abrasive flow rate, M_a	0.71
Cutting quality (1 = min, 5 = max), q	5
Mixing tube diameter, d_m	0.030
Constant, C	163

Table 1 Abrasive waterjet machining settings used in cost model.

The cutting path in a typical abrasive waterjet manufacturing job is not linear. This issue requires a modification to the linear cutting speed estimation equation in order to estimate the cutting speed along cut curves with an arc section radius, u_{as}. This involves a modification to (7) using (9) to replace the quality factor, q. This modification takes into account the radius of curvature of the cut path, R. The resulting cutting speed estimation is shown in (10).

$$q = \frac{0.182h}{(R+E)^2 - R^2} \tag{9}$$

$$u_{max} = \left(\frac{f_a N_m P_w^{1.594} d_o^{1.374} M_a^{0.343} \left[(R+E)^2 - R^2 \right]}{0.182 C h^2 d_m^{0.618}} \right)^{1.15} \tag{10}$$

In (9) and (10), E is the error limit. When the waterjet traverses a curve or executes a sharp corner, the lag causes an error in following the true line because the exit point at the bottom of the material is not above the entry point at the top of the material. As the traverse speed is lowered, the lag and the associated error is reduced. The user-defined error limit is related to the quality level for the surface of the cut. From Olsen (1996), the appropriate error limit of 0.001 is used with respect to the desired cutting quality.

Total manufacturing cost is estimated using (11).

$$C_{man} = OC \left[\sum_{i=1}^{m} \left(\sum_{j=1}^{\mathbf{s_i}} \frac{\mathbf{L_j}}{u_{(i,j)}} \right) \right] \tag{11}$$

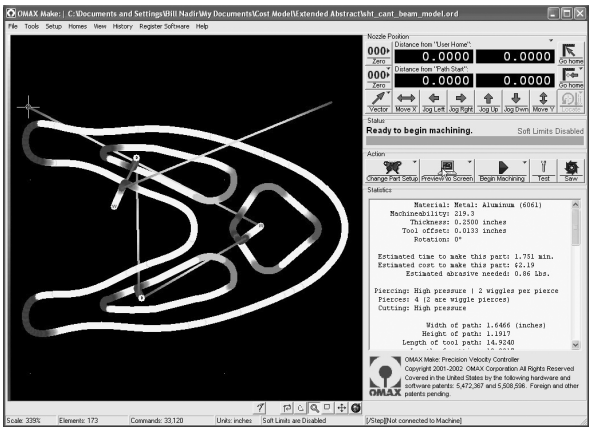

Fig. 2 Omax output screenshot for short cantilevered beam example.

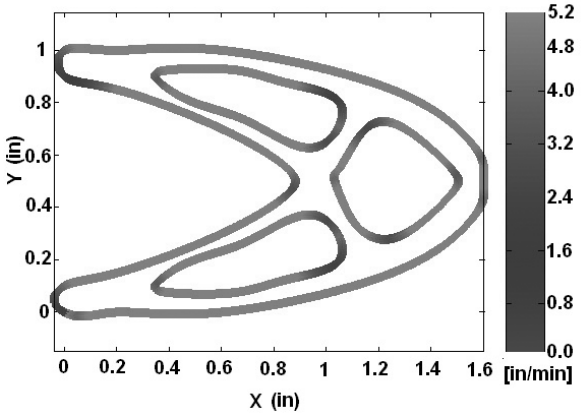

Fig. 3 MATLAB AWJ cost model output for short cantilevered beam example.

In (11), L_j is the length of the j^{th} step along the cutting curve, u is the AWJ cutting speed for the i^{th} step along the j^{th} curve, either arc section or maximum linear cutting speed, m is the maximum number of closed curves, and $\mathbf{s_i}$ is the total number of steps along the cutting curve for the i^{th} curve.

In order to validate the manufacturing cost estimation model, results from the model are compared to Omax results for a short cantilevered beam manufacturing scenario. Omax contains an accurate manufacturing cost estimator and is a good benchmarking tool for this application. A screenshot of the Omax result is shown in Figure 2. Figure 3 is the output of the MATLAB AWJ cost estimation model.

The results of the software validation shown in Table 2 show the MATLAB manufacturing cost estimation software accurately estimates manufacturing cost for abrasive waterjet cutting.

	Omax	Cost Model
Manufacturing Time (min)	1.69	1.71
Manufacturing Cost	$2.14	$2.11

Table 2 Manufacturing cost estimation module validation results.

2.8 Structural analysis module

The structural analysis software is linked to MATLAB for the optimization process. Required inputs to this module are the material properties, geometrical definitions for the structure, degree of freedom constraints for the structure, and load vectors applied to the structure. Outputs obtained from the module are the maximum von-Mises stress and the structural volume. These outputs are used to evaluate the objective function and determine if the structural design satisfies the constraints.

3 Example 1: Generic Part Optimization

The first example presented is mass versus manufacturing cost optimization for a simple structural part. Visualization of the design variable side constraints for the shape control points is shown in Figure 4. The grey areas denote zones in which the three sets of four shape control points are free to move.

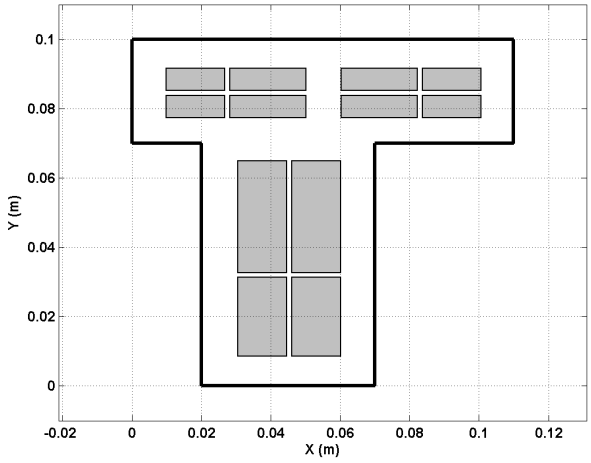

Fig. 4 Side constraints of the shape control points for generic structural part optimization example.

It can be seen in Figure 4 that the side constraints restrict the simulated abrasive waterjet cuts to be internal to the part. The side constraints for this example are restricted to the zones shown in order to prevent NURBS

curves from intersecting each other or with the boundary of the part. If any of these intersections were to occur, the ANSYS structural analysis module would not be able to mesh the part and compute a solution.

3.1 Optimization procedure

MATLAB modules were created to perform the structural optimization for manufacturing cost and structural performance for this example. These routines include a main software module, an AWJ manufacturing cost estimation module (Section 2.7), and a structural analysis module (Section 2.8). Important parameters and initialization techniques associated with each software module for this design example are presented in this section.

3.1.1 Simulation parameters

The important parameters set in this module are the geometry of the structural component, the number of initial designs to consider, objective function weighting factors, material properties of the truss structure elements, and abrasive waterjet settings. For this structural design example, the geometry defining the boundary of the part is defined. These properties are presented in Section 2.4. Three different initial designs were selected for the simulations. This is explained in more detail in Section 3.1.2. The material properties are defined in this module as well. The material selected is A36 Steel with a Young's modulus of 200 GPa, a Poisson's ratio of 0.26, and a yield strength of 250 MPa. The abrasive waterjet settings used are defined in Section 2.7.

The material thickness of the part is assumed to be 1 centimeter. The boundary conditions of the part are designed such that the part is fixed in all directions at the base as shown in Figure 5. The evenly-distributed pressure across the top of the part, also shown in Figure 5, is $3.7\text{x}10^7 N/m^2$. A factor of safety of 1.5 is assumed for this example.

Three holes are cut in the metallic part and the shapes of these holes are controlled by four control points each. These control points are illustrated in Figure 6. The cutting path created by the control points is determined using NURBS curves created in ANSYS using the *spline* command.

In this example, objective function weighting factors of 0.2, 0.6, 0.65, 0.7, 0.75, 0.8, 0.85, 0.9, and 0.95 are used. The criteria used for selecting the weighting factors is explained in Section 3.2.3.

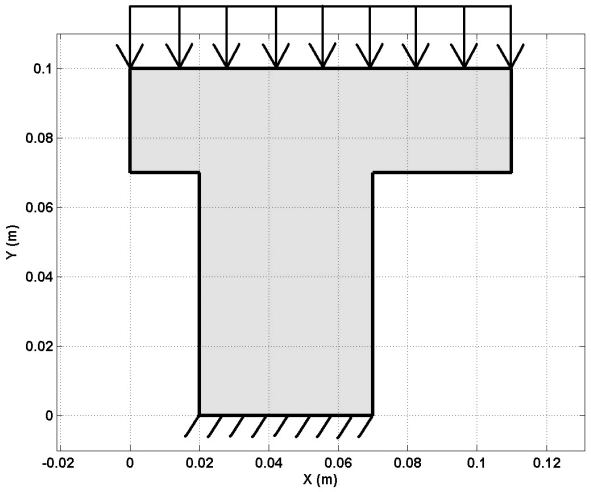

Fig. 5 Generic structural part design including loading and boundary conditions.

3.1.2 Initialization

This design optimization example is performed by starting the optimization algorithm at three different initial designs. Optimization is performed by first defining an initial structural solution guess. These three designs are selected to attempt to broadly search the design space with the goal of finding solutions close to the global optimum. The initial designs for the example, shown in Figure 6, include small, medium, and large holes cut in the blank metallic part.

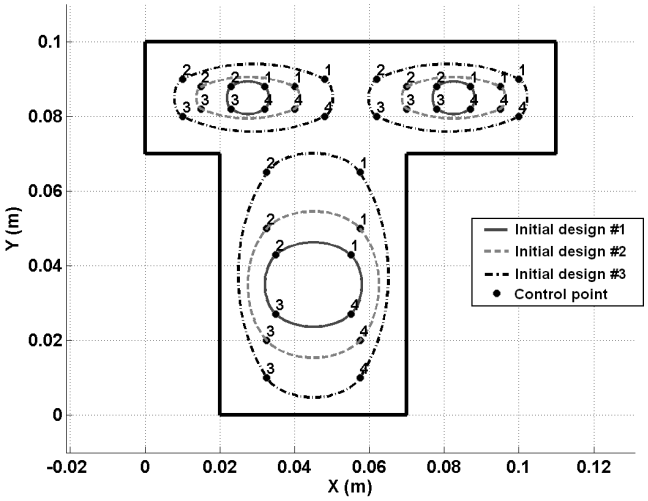

Fig. 6 Initial designs for the generic structural part shape optimization example.

The goal of starting the optimization with many different initial guesses is to attempt to find a near-global optimal solution. A gradient-based optimization method, used for the outer loop of this optimization framework, has a tendency to get trapped at a local optimal solution. By starting the optimization routine from several different locations in the design space, there is a greater potential for finding a near-optimal solution.

3.2 Results

Structural component shape optimization considering both performance and manufacturing cost is performed for a generic metallic structural part shown in Figure 5.

3.2.1 Objective space results

Pareto frontier results for shape optimization for this example are shown in Figure 7. The maximum von-Mises stress constraint is active for all designs along the Pareto frontier except the results for weighting factors of 0.2 and 0.6.

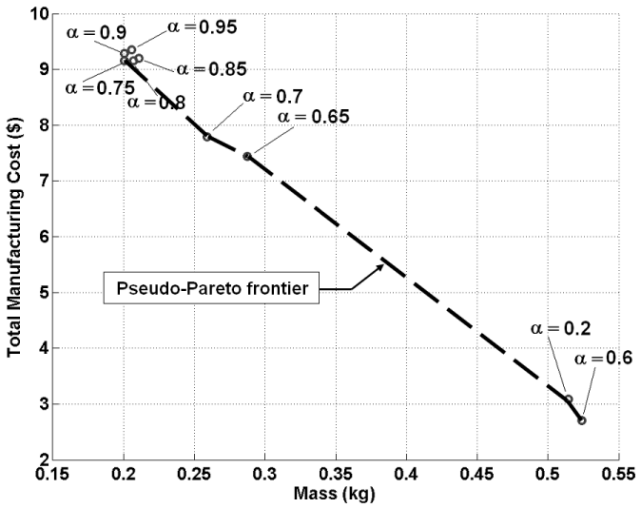

Fig. 7 Objective space results for generic part optimization with objective function weighting factor, α, labeled for each design.

An evenly distributed Pareto frontier is not found in this multiobjective optimization. This phenomenon is likely caused by the fact that the objectives being minimized are highly nonlinear in terms of the weighting factor, α, and an even distribution of weighting factors is not the best method to find the Pareto front. The use of the adaptive weighted-sum (AWS) method by Kim and de Weck (2005) may alleviate this problem and will be implemented in future work. In order to attempt to overcome this difficulty, a select set of weighting factors is chosen to attempt to obtain a well-distributed Pareto frontier. As can be seen in Figure 7, even this select set of weighting factors does not yield such a Pareto frontier.

Although the Pareto frontier is not well-distributed, the trade-off between mass and manufacturing cost can be seen. A pseudo-Pareto frontier is denoted by connecting all the non-dominated design solution points because the actual Pareto frontier is not known given the design solutions obtained.

3.2.2 Design space results

Selected structural designs from the set from Figure 7 are shown in Figures 8, 9, and 10.

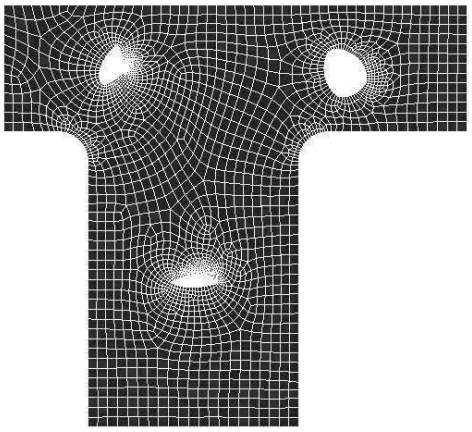

Fig. 8 Weighting factor of 0.6.

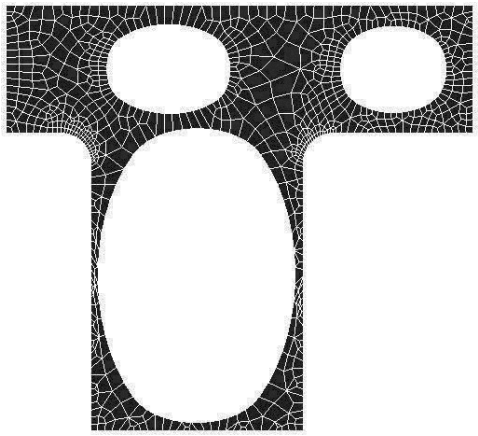

Fig. 9 Weighting factor of 0.7.

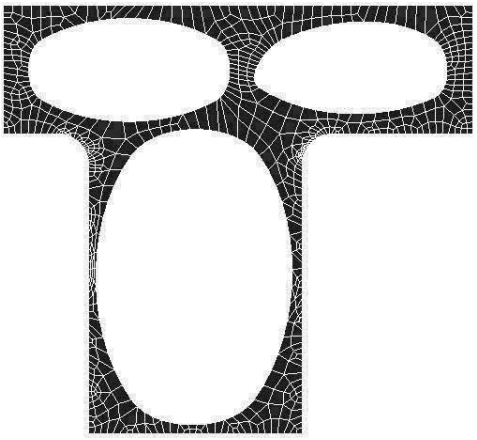

Fig. 10 Weighting factor of 0.9.

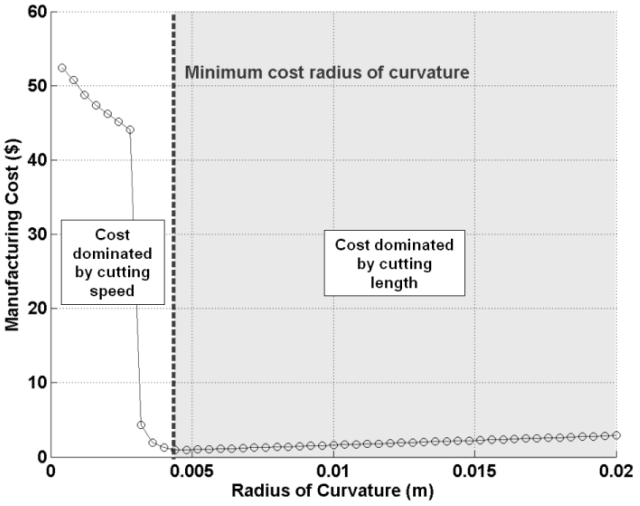

Fig. 11 Manufacturing cost vs. radius of curvature for circular cuts.

The structural design results demonstrate the trade-off between cost and mass. When manufacturing cost is weighted more heavily, the cut-outs in the metallic part are small. However, when mass is weighted more heavily, the cut-outs in the part are significantly larger and one or more of the holes are at or near the side constraint boundaries. This means the optimization algorithm is attempting to remove material to minimize structural mass, as expected.

3.2.3
Objective space results discussion

It is observed that the weighted sum design solutions are not in the expected order. The solution from the weighting factor of 0.2 should have lower cost and greater mass than the solution for the weighting factor of 0.6, yet this is not the case. There are two likely causes for this problem. First, it is possible that too few initial designs are investigated in order to find a near-global optimal design solution. The design solutions found are likely local optima and not global optimal solutions. However, a more likely cause of this problem is that manufacturing cost is not only a function of cutting curve length but also the radius of curvature of the cutting path. As mentioned previously, in the manufacturing cost model, a specific cutting path radius of curvature limit exists at which cuts with radii greater than the limit are assumed to be at the maximum cutting speed. As shown in Figure 11, below this radius of curvature limit, cutting speed is slower and not constant and therefore the cost per unit length of material increases.

Figure 11 illustrates this radius of curvature limit for manufacturing cost minimization. The example used to illustrate this phenomenon is a comparison of closed circular cuts with varying radii. Figure 11 shows the minimum manufacturing cost with respect to radius of curvature. A clear minimum manufacturing cost can be seen at the limit of the maximum linear cutting speed. This minimum was obtained from observations of the radius of curvature limit at which Omax software assumed the maximum linear waterjet cutting speed was used for various cutting qualities. Two important trends can be seen in Figure 11. First, when the radius of curvature is less than the minimum cost radius of curvature, cutting speed dominates the manufacturing cost. This results in a dramatic rise in manufacturing cost for small reductions in radius of curvature. For radii of curvature larger than the minimum cost radius, cost is dominated by cutting length. This leads to an increase in manufacturing cost with a linear relationship to radius of curvature.

3.2.4
Convergence information

The convergence histories for the optimizations performed for each weighting factor are shown in Figure 12. The convergence rate is dependent on the objective function weighting factor and ranges from two to thirty-eight iterations. As shown in the figure, starting the optimization from an infeasible region does not prevent the optimizer from finding feasible designs and converging. In Figure 12, for infeasible initial designs, the change to the feasible design region is noted.

4
Example 2: Bicycle Frame Optimization

This section includes the same optimization algorithm applied to a more complex structural component design example. This component is a two-dimensional bicycle frame-like structure. The design objectives for this example are the same as those for the generic part opti-

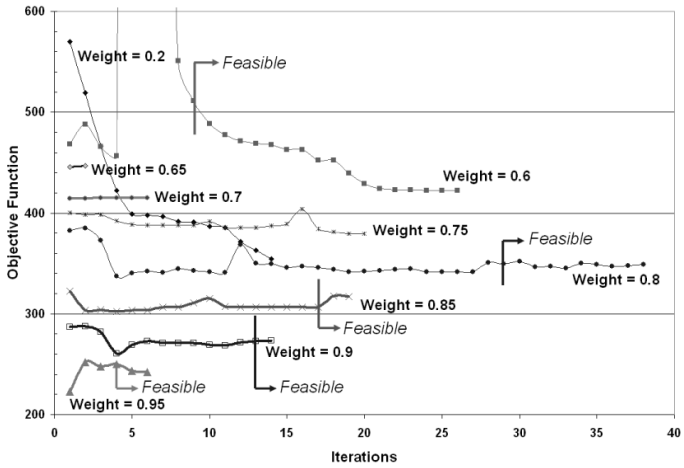

Fig. 12 Convergence histories for the generic part structural optimization example.

mization example (see (1)). The design variables for the simulation for this example are identical to those presented in Section 2.3.

4.1 Design constraints

The constraints imposed on this problem statement are X, Y location shape constraints of the design variables and maximum von-Mises stress in the structure. These constraints are defined in (4), (5), and (6). Shape design variable constraints are shown in Figure 13.

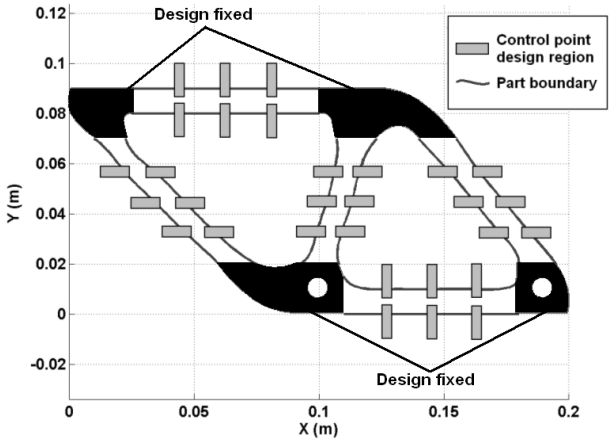

Fig. 13 Shape design constraints of the control points for bicycle frame design optimization example.

Figure 13 illustrates how the simulated abrasive waterjet cuts form large portions of the part boundary. The control point shape constraints are restricted to the zones shown in order to prevent any of the resulting NURBS curves from intersecting each other.

4.2 Optimization procedure

The same optimization procedure presented for Example 1 is used for this design example. Differences in the design example problem setup are presented in this section.

4.2.1 Parameters

For this example, the boundaries of the portions of the structure not being optimized are predefined. These properties are presented in Section 4.1. Three different initial designs were selected for the simulations. This is explained in more detail in the following Initialization section. The material properties and abrasive waterjet settings for this design example are the same as Example 1.

For this example, an evenly distributed set of eleven weighting factors between 0 and 1 are used. The criteria used for selecting the weighting factors is explained in Section 4.3.2.

4.2.2 Initialization

Design optimization is performed by starting the optimization algorithm at three different initial designs as was done for Example 1. These initial designs are shown in Figures 14, 15, and 16. The bicycle frame structures have thin, medium, and thick-sized structural members. A near-global optimum design is found by selecting the best design of the three optimized solutions resulting from the three different initial designs. These best design solutions are used to create the Pareto frontier.

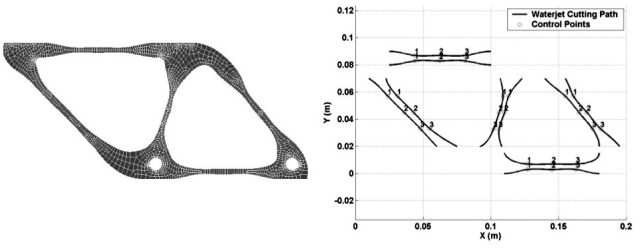

Fig. 14 Thin structural member initial design mesh and control points for bicycle frame structural optimization example.

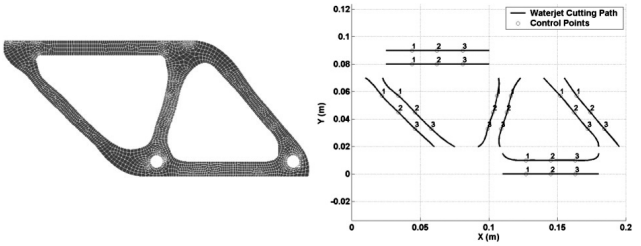

Fig. 15 Medium thickness structural member initial design mesh and control points for bicycle frame structural optimization example.

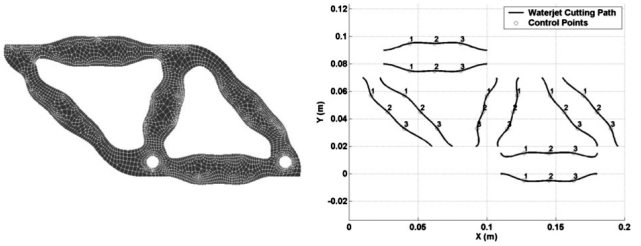

Fig. 16 Thickest structural member initial design mesh and control points for bicycle frame structural optimization example.

4.3 Results

Shape optimization considering both structural performance and manufacturing cost is performed for a bicycle frame-like part shown in Figure 17. The size of the structure is roughly 20 cm width by 10 cm height.

4.3.1 Simulation parameters

The material thickness of the part is 1 centimeter. The loads and restraints are shown in Figure 17. A factor of safety of 1.5 is assumed.

Ten curves controlled by three control points each are used to determine the shape of the structure while the structural shape at the vertices of the structure remain unchanged. The relationship of the control points to the curves are shown in Figures 14, 15, and 16.

4.3.2 Objective space results

The Pareto frontier shown in Figure 18 demonstrates the trade-off between manufacturing cost and mass. The magnitude of improvement in manufacturing cost along the Pareto frontier is not large. For this example, a manufacturing cost savings of approximately 1.6% is observed

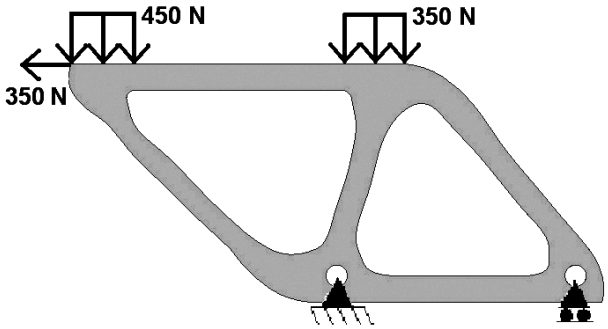

Fig. 17 Structural part design with loading and boundary conditions shown.

when comparing the two anchor points of the Pareto frontier. However, a small improvement in manufacturing cost applied to a product being mass produced can result in a large cost savings for a manufacturer. In addition, the observed trade-off between cost and mass would be more significant if the shapes of the bicycle frame joints are included in the design space. Since large portions of the structure are fixed, the design space and therefore the cost and mass trade-off is restricted.

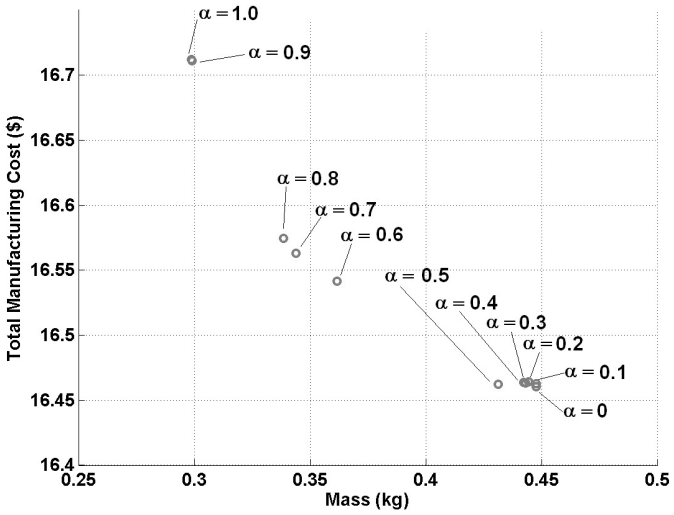

Fig. 18 Pareto frontier for bicycle frame structural optimization with weighting factor, α, labeled for each design.

The maximum von-Mises stress constraint is not active for any of the structural designs included in the Pareto frontier. This is a result of the control point X, Y constraints being restrictive. Design freedom is limited by these constraints in order to prevent part edge curves from intersecting each other, resulting in designs for which structural analysis cannot be performed.

Abrasive waterjet cutting speeds for all designs for this example are determined to be at the maximum lin-

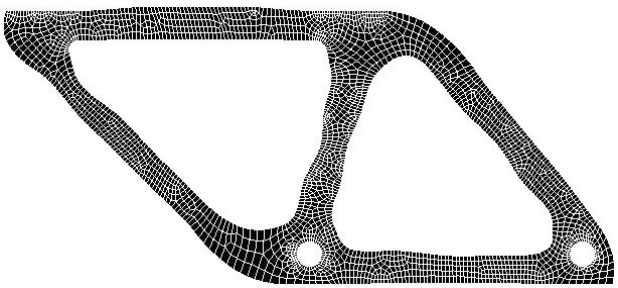

Fig. 19 Structural design solution for weighting factor of 0.1.

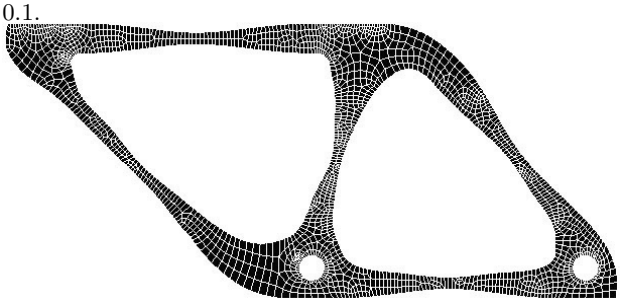

Fig. 20 Structural design solution for weighting factor of 0.6.

ear cutting speed of the AWJ cutter for the selected example. This results in better objective space results than are obtained for the generic structural part example presented in Section 3.2.1.

4.3.3 Design space results

Selected structural designs from the Pareto set are shown in Figures 19 and 20. The trade-off between objectives can be seen by comparing structural designs for these weighting factors. The design for which the weighting factor is 0.1 results in a structure with nearly straight edges for minimum manufacturing cost. However, the design for a weighting factor of 0.6 results in a design with narrow structural members in order to minimize structural mass. This results in low mass but higher manufacturing cost as a result.

5 Conclusions and Future Work

While the area of structural shape optimization is fairly mature, we introduce in this paper the consideration of manufacturing cost in the optimization process. Although a two-dimensional manufacturing process, abrasive waterjet cutting, is selected for this paper, other more complicated manufacturing processes can be used as well. Two examples are used to exemplify the application of this procedure for multiobjective structural optimization problems.

The trade-off between structural performance and manufacturing cost is shown with Pareto frontiers for two example structural components. Mass is used as the metric for structural performance and maximum von-Mises stress is the constraint.

Future work will include implementing the adaptive weighted sum (AWS) method developed by Kim and de Weck (2005) for the generic structural part example. This method may allow for the generation of a well-distributed Pareto frontier for the example. The bicycle frame example results will be improved by including the bicycle frame joints in the design space by allowing their shapes to be optimized. Additional future work will include performing topology optimization in which the number of curves are considered as design variables and the creation and merging of holes is allowed. Finally, the method will be applied to more complex structures and a new manufacturing cost model will be implemented. Potential manufacturing process cost models could include milling and stamping.

References

Bendsøe, M. O.; Kikuchi, N. 1988: Generating optimal topologies in structural design using a homogenization method. *Comput. Methods Appl. Mesh. Eng.*, **71**, 197-224.

Chang, K. H.; Tang, P. S. 2001: Integration of design and manufacturing for structural shape optimization. *Adv. Eng. Softw.*, **32**, 555-567.

Curran, R. et. al. 2005: Integrating Manufacturing Cost and Structural Requirements in a Systems Engineering Approach to Aircraft Design. *Proceedings of the* 46^{th} *AIAA/ASME/ASCE/AHS/ASC Structures, Structural Dynamics & Materials Conference*, Austin, Texas.

Haug, E. J. et. al. 1986: *Design sensitivity analysis of structural systems*, Academic Press, San Diego, California.

Kim, I. Y.; Kwak, B. M. 2002: Design Space Optimization Using a Numerical Design Continuation Method. *Int. J. Numer. Meth. Eng.*, **53**, 1979-2002.

Kim, I. Y.; de Weck, O. L. 2005: Adaptive Weighted Sum Method for Bi-objective Optimization: Pareto front generation. *Struct. Multidisc. Optim.*, **29**, 149-158.

Kim, I. Y.; de Weck, O. L. 2005: Variable chomosome length genetic algorithm for progressive refinement in topology optimization. *Struct. Multidisc. Optim.*, **29**, 445-456.

Koski, J. 1988: Multicriteria truss optimization. In: Stadler, W. (ed.), *Multicriteria Optimization in Engineering and in the Sciences*, Plenum Press, New York, New York.

Lee, S. B. et. al. 2004: Continuum Topology Optimization. *Proceedings of the* 10^{th} *AIAA/ISSMO Multidisciplinary Analysis and Optimization Conference*, Albany, New York.

Martinez, M. P. et. al. 2001: Manufacturability Based Optimization of Aircraft Structures Using Physical Programming. *AIAA Journal*, **39**, 517-525.

Olsen, J. 1996: *Motion Control with Precomputation*, U.S. Patent 5,508,596, Assignee: Omax Corporation.

Park, C. et. al. 2004: Simultaneous optimization of composite structures considering mechanical performance and manufacturing cost. *Compos. Struct.*, **65**, 117-127.

Piegl, L.; Tiller, W. 1997: *The NURBS Book*, Springer Verlag, Heidelberg, Germany.

Singh, P.; Munoz, J. 1993: Cost Optimization of Abrasive Waterjet Cutting Systems. *Proceedings of the* 7^{th} *American Water Jet Conference*, Seattle, Washington, 191-204.

Suzuki, K.; Kikuchi, N. 1991: A homogenization method for shape and topology optimization. *Comput. Methods Appl. Mech. Eng.*, **93**, 291-318.

Yang, R. J.; Chuang, C. H. 1994: Optimal topology design using linear programming. *Comput. Struct.*, **52**, 265-275.

Zadeh, L. 1963: Optimality and Non-Scalar-Valued Performance Criteria. *IEEE Trans. Automat. Contr.*, **8**, 59-60.

Zeng, J. 1992: *Mechanisms of Brittle Material Erosion Associated with High-pressure Abrasive Waterjet Processing*, PhD thesis, University of Rhode Island, Department of Mechanical Engineering and Applied Mechanics.

Zeng, J. et. al. 1992: Quantitative Evaluation of Machinability in Abrasive Waterjet Machining. *Precision Machining: Technology and Machine Development and Improvement at the Winter Annual Meeting of The American Society of Mechanical Engineers*, Anaheim, California, 169-179.

Zeng, J.; Kim, T. 1993: Parameter Prediction and Cost Analysis in Abrasive Waterjet Cutting Operations. *Proceedings of the* 7^{th} *American Water Jet Conference*, Seattle, Washington, 175-189.

Zeng, J. et. al. 1999: The Abrasive Water Jet as a Precision Metal Cutting Tool. *Proceedings of the* 10^{th} *American Water Jet Conference*, Houston, Texas, 829-843.

Zolésio, J. P. 1981: Multicriteria truss optimization. In: *Optimization of Distributed Parameter Structures*, Sijthoff & Noordhof, The Netherlands.